Lymphatic dysfunction in lupus contributes to cutaneous photosensitivity and lymph node B cell responses

William G. Ambler[1,2,†], Mir Howlander[1,3], Madhavi Latha S. Chalasani[1,3,‡], Ethan S. Seltzer[1], JiHyun Sim[1,3], Jinyeon Shin[4], Noa Schwartz[1,5, §], William D Shipman III[1,3§§], Dragos Dasoveanu[1,6,††], Camila B. Carballo[7], Ecem Sevim[5,¶], Salma Siddique[2,5,¶¶], Scott Rodeo[7,8], Doruk Erkan[5], Raghu P. Kataru[4], Babak Mehrara[4], Theresa T. Lu[1,2,3,5]*

[1]Autoimmunity and Inflammation Program, Hospital for Special Surgery Research Institute; New York, NY, USA

[2]Pediatric Rheumatology, Department of Medicine, Hospital for Special Surgery; New York, NY, USA

[3]Department of Microbiology and Immunology, Weill Cornell Medicine; New York, NY, USA

[4]Division of Plastic and Reconstructive Surgery, Department of Surgery, Memorial Sloan Kettering Cancer Center; New York, NY, USA

[5]Rheumatology, Department of Medicine, Hospital for Special Surgery; New York, USA

[6]Physiology, Biophysics, and Systems Biology Graduate Program, Weill Cornell Medicine, New York, NY USA

[7]Orthopedic Soft Tissue Research Program, Hospital for Special Surgery Research Institute; New York, NY, USA

[8]Department of Orthopedics, Hospital for Special Surgery; New York, NY, USA

[†]Current address: Systemic Autoimmunity Branch, NIAMS/NIH, 10 Center Drive, 12N248C, Bethesda, Maryland, USA

[‡]Current address: Mnemo Therapeutics; Princeton, NJ, USA

[§]Current address: Department of Medicine (Rheumatology), Albert Einstein College of Medicine/Montefiore Medical Center; Bronx, NY, USA

[§§]Current Address: Department of Dermatology, Yale University; New Haven, CT, USA

[¶]Current address: Department of Rheumatology, NIAMS/NIH; Bethesda, MD, USA

[††]Current address: Department of Cancer Immunology, Genentech; South San Francisco, CA, USA

[¶¶]Current address: Nemours Hospital for Children, Wilmington, DE, USA

* Corresponding author:
Theresa T. Lu
Telephone: 212-774-2532
Email: lut@hss.edu

ABSTRACT

Photosensitivity in lupus and subsequent systemic disease flares contribute to disease burden and is incompletely understood. Skin communicates with lymphoid tissues via lymphatics and reduced lymphatic flow in murine models results in skin inflammation and autoimmunity. Here, we demonstrate that the skin of lupus patients and multiple murine lupus models are characterized by lymphatic flow dysfunction. Improving lymphatic flow in murine lupus models via manual lymphatic drainage or by utilizing a transgenic model with increased lymphatics ameliorated cutaneous photosensitivity and diminished draining lymph node germinal center B cell and plasmablast responses. Improved lymphatic flow limited B cell responses via acting on a stromal-immune circuit previously described by our lab. Increased lymphatic flow increases stromal CCL2, which modulates monocyte function and limits B cell responses. This work provides a link between cutaneous photosensitivity and systemic disease in lupus and suggests that improving lymphatic flow or targeting the lymph node microenvironment could be potential therapeutic targets.

INTRODUCTION

In patients with the autoimmune disease systemic lupus erythematosus (SLE), ultraviolet radiation (UVR) from sunlight can trigger both the development of inflammatory skin lesions and flares of systemic disease, resulting in increased autoantibody levels, further end organ injury, and patient morbidity. Currently, medications used for photosensitive skin responses include topical steroids, topical calcineurin inhibitors, and antimalarials such as hydroxychloroquine. More importantly, lupus patients are advised to reduce UVR exposure by avoiding the sun, wearing protective clothing, and wearing sunscreen to prevent photosensitive skin responses and their sequelae [1-3]. Photosensitive skin inflammation, the accompanying risk of systemic disease flares, and the lifestyle modifications needed to prevent these all contribute to disrupting patients' quality of life [4-6]. Advances have begun to delineate the mechanisms that contribute to photosensitivity [7-9]. However, how skin sensitivity to UVR is connected to increased autoimmunity remains poorly understood.

Skin communicates with lymphoid tissues via lymphatic vessels which transport cells and interstitial fluid to skin-draining lymph nodes where immune responses occur and can be regulated. This lymphatic transport serves both to clear fluid and inflammation from the skin and to deliver antigens, antigen-presenting cells, and mediators that impact lymph node function. Reduced lymphatic flow results in skin inflammation and, over time, spontaneous autoantibody generation [10, 11], a scenario that is reminiscent of SLE and suggests the possibility of lymphatic dysfunction in SLE.

How skin signals may regulate lymph node immune responses in SLE is poorly understood, but fibroblastic reticular cells (FRCs) that comprise the lymph node stromal infrastructure are among the first sensors of afferent lymph. FRCs are increasingly appreciated

for their roles in modulating immune responses, and we recently delineated an FRC CCL2 axis whereby FRC-derived CCL2 is upregulated and regulates Ly6C^{hi} monocytes that limit plasmablast survival in immunized mice [12]. Input from the skin to the lymph node that regulates FRC CCL2, then, could impact lymph node B cell responses.

In this study, we examined for lymphatic dysfunction in both human SLE and murine SLE models and sought to understand the consequences on both skin and lymph node function. Our data show evidence of compromised lymphatic flow in human SLE and multiple SLE models. Improving lymphatic flow by manual lymphatic drainage or in a transgenic model with increased lymphatics reduced UVR-induced skin inflammation and B cell responses in draining lymph nodes. We further show that improving flow upregulates FRC CCL2, driving the FRC-monocyte axis to limit B cell responses. These results suggest that lymphatic flow is compromised in SLE and that this dysfunction contributes to both cutaneous photosensitivity and lymph node B cell activity in disease. This scenario suggests that improving lymphatic flow may be therapeutically useful in SLE.

RESULTS

We assessed for lymphatic flow alterations in the skin of human SLE and SLE mouse models. Human skin lymphatic vessels show a dilated phenotype when lymphatic flow is compromised [13-15]. Patients with SLE, patients with persistently positive antiphospholipid antibodies (APL), and patients with concomitant SLE and APL can have a lacy pattern of prominent veins on the skin, especially noticeable on the forearms [16]. Biopsies of the pale areas of the skin among the veins showed that patients with SLE had dilated lymphatic vessels when compared to patients with APL without SLE, which was similar to two healthy controls **(Figure 1A-B**). There was no change in the density of lymphatic vessels **(Figure 1C).** These results showing dilated lymphatics in SLE compared to patients without SLE suggested that there is dysfunctional lymphatic flow in SLE.

We examined lymphatic flow by assaying for retention of intradermally injected Evans blue dye [17] in two photosensitive lupus models, the MRL-*Fas*^{lpr} (LPR) spontaneous lupus model and an inducible lupus model using chronic epicutaneous imiquimod on a B6 background (B6 IMQ) [18-20]. UVR treatment of LPR mice without discernable skin disease led to increased Evans blue retention that corresponded to the greater skin swelling when compared to UVR-treated MRL-MpJ (MRL) controls **(Figure 1D-F)** while MRL and LPR mice showed no differences at baseline **(Figure 1G-H)**.

For the IMQ model, we applied IMQ on the right ear, generating a “lesional” ear, leaving the skin on the rest of the body, including the left ear, as “non-lesional” skin. Both the non-lesional and lesional ears showed increased Evans blue retention with increased skin swelling upon UVR exposure when compared to control B6 mice **(Figure 1I-K)**. Together, these findings

in two distinct SLE models support our findings in human SLE that there is compromised skin lymphatic flow in SLE.

We asked about the contribution of reduced lymphatic flow to photosensitivity in the SLE models by using two different approaches to improve lymphatic flow. Manual lymphatic drainage (MLD) is used to reduce swelling in patients with acquired or congenital lymphedema [21, 22], and we adapted this procedure to mice. MLD targeted at the left ear was administered once a day during the course of UVR exposure **(Figure 2A)**, and this treatment decreased Evans blue retention in LPR mice relative to handling controls **(Figure 2B-C)**, suggesting that MLD was successful in improving lymphatic flow. MLD also ameliorated UVR induced skin inflammation, with reduced ear swelling, reduced monocyte and T cell accumulation, and a trend toward reduced neutrophil accumulation **(Figure 2D-G)**. MLD had similar effects in IMQ mice **(Figure 2H-M)**. Thus, MLD in both the LPR and IMQ SLE models ameliorated photosensitivity.

B6 PTEN$^{fl/fl}$ Flt4Cre^{ERT2} mice treated with tamoxifen (LEC^{PTEN} mice) have PTEN, an antagonist of critical VEGFC/VEGRF3 signaling, deleted in LECs, which results in expansion of functional lymphatic vessels, improved lymphatic flow from skin, and reduced UVR-induced skin inflammation in healthy (ie non-lupus) mice [23]. We induced the IMQ model in LEC^{PTEN} mice and LEC^{WT} controls to generate IMQ-LEC^{PTEN} mice and IMQ-LEC^{WT} mice (**Figure 2N**). Reduced Evans blue retention in both non-lesional (left) and lesional (right) ears of IMQ-LEC^{PTEN} mice compared to IMQ-LEC^{WT} controls confirmed improved lymphatic drainage (**Figure 2O**), and this was associated with reduced UVR-induced ear swelling and inflammation **(Figure 2P-S)**. Notably, tamoxifen treatment of WT mice did not reduce Evans blue retention or ear swelling **(Figure 2T-U)**, indicating that effects in IMQ-LEC^{PTEN} mice were attributable to

PTEN deletion rather than to tamoxifen treatment. Consistent with prior reports that improved lymphatic drainage can reduce cutaneous inflammation [24, 25], our results showed using both an acute physical approach and a long-term genetic approach that improving lymphatic flow from skin reduced cutaneous photosensitivity in SLE model mice.

We asked whether lymphatic flow alterations in SLE models contributed to modulating immune activity in downstream lymph nodes. Improving lymphatic flow during UVR exposure with MLD did not affect overall lymph node cellularity in draining auricular nodes (**Figure 3A**). MLD also did not alter B and T cell numbers, although there was a trend toward a reduced B:T cell ratio that may reflect reduced lymph node inflammation (**Figure 3B**) [12, 26]. Germinal center B cells along with CD138+intracellular IgG+ cells showing high percentages of ki67 expression indicating an active B cell response and plasmablast generation were present in lymph nodes draining "non-lesional" skin (28.9% +/- 19.2% CD138+intracellular IgG+ cells expressing ki67), and germinal center B cell and plasmablast numbers were decreased with MLD (**Figure 3C**). LPR mice, which despite altered lymph node architecture and large accumulation of double negative T cells characteristic of this model [27], similarly showed reduced germinal center B cells after MLD (**Figure S1**). These data suggested that even a short period of improved lymphatic flow can reduce B cell responses in the draining lymph node.

UVR-treated IMQ-LEC^{PTEN} mice showed decreased lymph node cellularity when compared to IMQ-LEC^{WT} mice (**Figure 3D**), with decreases in both B and T cells (**Figure 3E**). B cell decreases were greater than T cell decreases, resulting in a reduced B:T cell ratio (**Figure 3E**) and further suggesting reduced inflammation in lymph nodes [12, 26]. Germinal center B cell and plasmablast numbers were also decreased in the IMQ-LEC^{PTEN} mice (**Figure 3F**). The IMQ model of SLE develops significant splenomegaly [18, 28] and IMQ-LEC^{PTEN} mice had

reduced splenomegaly, demonstrating reduction in systemic disease activity (**Figure 3G**). This genetic model of chronic and generalized improved lymphatic flow showed reduced lymph node B cell responses, similar to MLD and, additionally, showed reduced systemic disease.

We recently described a regulatory axis in lymph nodes whereby fibroblastic reticular cells (FRCs) upregulated CCL2 after immunization, which altered monocyte function to limit plasmablast survival [12]. FRCs are among the early sensors of lymphatic flow into lymph nodes, and changes in fluid flow across FRCs have been shown to modulate FRC chemokine expression [29]. We thus asked if modulating FRC CCL2 could be a mechanism by which improving lymphatic flow reduced B cell responses. Upon MLD treatment of IMQ-treated CCL2-GFP reporter mice, FRCs showed upregulated CCL2 expression (**Figure 4A**). By anti-CCL2 staining, an increase in FRC CCL2 was also detectable in IMQ-LEC^{PTEN} mice compared with control IMQ-LEC^{WT} mice (**Figure 4B**). MLD also increased LEC CCL2 expression (**Figure 4C).** Although increased stromal CCL2 can potentially promote monocyte accumulation in lymph nodes, (CCR2-expressing) Ly6C hi monocytes did not show increased numbers with MLD (**Figure 4D**). Stromal CCL2 also modulated monocyte phenotype in immunized healthy mice, including increased ROS generation [12] and a reduced CD11b expression that was not related to cell size changes (**Figure 4E**). Similarly, the MLD-induced increase in FRC CCL2 was associated with reduced monocyte CD11b expression without concurrent cell size changes (**Figure 4F**), suggesting that the MLD-induced increase in stromal CCL2 affected monocyte function. Together, these results suggested that improving lymphatic flow increased stromal CCL2 and altered CCR2 monocyte function in draining lymph nodes.

We asked if monocytes were required for the reduced B cell responses seen with improved lymphatic flow. Monocyte depletion with anti-Gr-1 [12] in B6 IMQ mice during UVR and MLD

(**Figure 5A**) had no effect on lymph node cellularity but abrogated the MLD-induced increase in germinal center B cell and plasmablast numbers **(Figure 5B-D)**. These results suggested that improved lymphatic flow limits B cell responses in a monocyte-dependent manner, and together with the previous data, suggest a model whereby improving lymphatic flow in SLE model mice reduces draining lymph node B cell responses at least in part by upregulating FRC CCL2 and modulating monocyte function.

Discussion:

Lymphatic flow is critical for clearing inflammatory mediators from peripheral tissues and for communicating with draining lymphoid tissues, and here we show using human tissue and murine models that skin in SLE is characterized by lymphatic flow dysfunction. This lymphatic dysfunction contributed to both cutaneous photosensitivity and draining lymph node B cell responses in SLE models. Mechanistically, improving lymphatic flow from skin to lymph nodes increased lymph node stromal CCL2 to alter inflammatory monocyte phenotype to limit germinal center and plasmablast responses. Together, our data suggest that dysfunctional lymphatic flow is a contributing factor to lupus pathophysiology and points to lymphatic function as a therapeutic target.

In addition to providing a link between cutaneous photosensitivity and systemic disease activity in SLE, this work points to the lymph node stromal microenvironment as a potential therapeutic target. Further work will be needed to understand how improved lymphatic flow regulates FRC CCL2 expression and the extent to which there are other CCR2+ cells in addition to monocytes being modulated to limit B cell responses.

Our results showed that a 4-day course of MLD to improve lymphatic flow was able to reduce B cell responses in the draining lymph node. Although further analysis of effects of longer-term and perhaps MLD of multiple sites on systemic disease is needed, our current results suggest the possibility that MLD could be used as an immediately available and relatively inexpensive therapeutic approach to ameliorate disease in SLE.

METHODS

Study Design

The purpose of this study was to examine lymphatic function in the skin of photosensitive lupus mouse models and human lupus skin as well as the consequences of lymphatic manipulation on cutaneous photosensitivity and lymph node responses. Laboratory mice were used as subjects for experiments. Human skin sections were also analyzed. Evans blue lymphangiography was used to assess lymphatic flow and flow cytometry was used to identify and quantify cell numbers. For experiments, sample sizes of n=3-20 animals per condition were evaluated in 2 to 11 independent experiments.

Human Samples Staining and Imaging

FFPE section from skin biopsies of patients with SLE and persistently positive APL (as described in a recently published study [16]) were used to stain for lymphatic vessels. Patients in the study had active livedo reticularis and biopsies were taken from both the pale and purple areas. 5 patients had SLE, three of which had concomitant persistent positive antiphospholipid antibodies and 3 patients had persistent positive APL without SLE. Two healthy donors from archived samples were also used. Ethical approval for this study was obtained from Hospital for Special Surgery Institutional Review Board (IRB) (IRB number: 2015-256), where participants had signed written informed consents for both the initial study and for the subsequent study of skin biopsies. Each biopsy specimen was fixed in formalin, then dehydrated and embedded in paraffin.

Samples were paraffin embedded and the 5-µm paraffin sections were deparaffinized in xylene and rehydrated in graded alcohol series. After a final wash with distilled water, specimen slides were placed in boiling Antigen Unmasking Solution, Tris-based (#H3301, Vector Laboratories) for 15 minutes. Slides were briefly washed in water and thereafter in phosphate buffered saline-0.025% triton-X-100 prior to blocking non-specific binding sites with phosphate buffered saline-3% BSA for 30 minutes at room temperature. Double immunostaining was performed with 1:40 dilution of D2-40, lymphatic endothelial cell marker mouse monoclonal antibody (Cat# 916602, Biolegend) and 1:100 dilution of CD31/PECAM-1, endothelial cell marker rabbit polyclonal antibody (#NB100-2284, Novus Biologicals) overnight at 4°C. Dilutions of antibodies were prepared in phosphate-buffered saline containing 0.5% bovine serum albumin. After washing the slides with PBS-0.025% triton-x-100, endogenous peroxidase was inhibited by incubating slides in 3% H2O2 for 15 minutes in the dark. The sections were then washed in distilled water followed by wash buffer and incubated with alkaline phosphatase conjugated donkey anti-mouse and horse radish peroxidase conjugated donkey anti-rabbit secondary antibodies (both Jackson ImmunoResearch, West Grove, PA) at 1:100 dilution (prepared in tris buffered saline with 0.5% bovine serum albumin) for 1 hr at room temperature. The reaction was revealed with 3,3′-diaminobenzidine Substrate Kit for Peroxidase and fast blue substrate (both Sigma-Aldrich, St. Louis, MO for alkaline phosphatase. At the end of incubation slides were washed in TBS-0.025% triton-X-100 and finally mounted with Clear-Mount (Electron Microscopy Sciences, Hatfield, PA) and baked at 56C for 20 minutes. Whole imaging was performed with Leica Aperio CS2 slide scanner (Deer Park, IL) at 40X magnification and analysis was done with ImageJ (NIH) analysis software. Lymphatic endothelial cells were visualized by double staining

for both D2-40 and CD31. Identification of lymphatic vessels were performed blinded to the patient diagnosis.

Mice

Mice between 6-12 weeks were used unless otherwise specified. Both male and female mice were used for experiments. All experiments were performed with age and sex matched controls. C57Bl/6, CCL2$^{-/-}$ [30], CCL2-GFP [31], MRL^{MpJ}, MRL-Fas^{lpr}, were originally from Jackson Laboratory (JAX, Bar Harbor, Maine) and bred at our facility. PTEN$^{fl/fl}$ CreERT2 [32] were generously provided by Babak Mehrara (Memorial Sloan Kettering, New York, NY). All animal procedures were performed in accordance with the regulations of the Institutional Animal Care and Use Committee at Weill Cornell Medicine (New York, NY).

Manual lymphatic drainage (MLD)

This technique was adapted to the mouse with the help of a licensed physical therapist with experience in MLD. MLD is performed locally on the left side in all experiments. This is performed daily for the number of days specified in each experiment. ProDerma smooth, powder-free latex gloves (Uniseal, Alhambra, CA) were used to minimize friction and cutaneous trauma. Mice are anesthetized and placed in a nose cone to sustain anesthesia throughout procedure. All movements were done at a speed of 1-2 seconds per movement. The mouse is initially placed supine, and the left forelimb is held by the paw and 20 circular clockwise rotations are performed. Circular movement with light pressure with the index finger is applied

to different lymph node groups. First the left submandibular area is done, followed the auricular area. After these circular movements the mouse is placed in the right lateral decubitus position and the left ear is held gently with a pincer grip (thumb and index finger). 50 light sweeping movements on the surface of the ventral ear distally to proximally are done with index finger. The mouse is then placed prone, and the ear is held again gently with a pincer grip. Small sweeping movements are done distally to proximally on the dorsum of the base of the ear (where the large collecting lymphatic vessels are and can be visualized by Evan's blue lymphangiography). 200 of these sweeping movements are done. The mouse is once again placed in the right lateral decubitus position and 20 sweeping movements at the base of the ear toward the auricular lymph node are done. The mouse is placed supine again and 20 circular movements of the left forelimb are repeated. Controls for MLD were anesthetized in the same manner and anesthesia was maintained in the nose cone. The mouse is placed prone, and the left ear is held with a pincer grip similarly to MLD. This is held for five minutes.

Mouse treatments

For UVR treatments, mice were exposed for four consecutive days using a bank of four FS40T12 sunlamps, as previously described [20]. MRL^{MpJ} and $MRL\text{-}Fas^{lpr}$ were exposed to 250 J/m^2/day for 4 days and C57Bl/6 mice were exposed to 333 J/m^2/day for 4 days. To measure ear swelling after UVR exposure, a caliper (Mitutoyo, Aurora, IL) was used. Each ear was measured in approximately the same location in the anterior half of the ear three times and the average was taken.

For the imiquimod (IMQ)-induced lupus mouse model, mice were painted on the dorsal and ventral sides of the right ear with 5% imiquimod cream (Taro Pharmaceutical, Hawthorne, NY) 3x/week for 4-5 weeks (~50 mg/mouse total cumulative dose) [18] prior to and continued through experiments.

To induce Cre-driver lines or to control for tamoxifen use, intraperitoneal (IP) tamoxifen (Sigma-Aldrich, CAS # 10540-29-1) was injected at a dose of 300mg/kg/day every other day for three doses. Tamoxifen was dissolved into 1.25 mL ethanol and 18.75mL corn oil 900mg of Tamoxifen by shaking overnight at 37°C.

For monocyte depletion studies, anti-Gr1 IgG antibody (RB6-8C5 cat#BE60075) or isotype control IgG (LTF-2, 2A3 cat#BE0090) were used (both BioXCell, West Lebanon, NH). Each antibody was injected IP at a dose of 250μg in 200μl PBS on indicated days.

Evan's blue lymphatic assay

Evan's blue retention assay was performed as previously described [33]. Mouse ears were injected intradermally using a Hamilton syringe (#1701, 10 ul syringe) with a 30-gauge needle. 1μl of 2% Evans blue (Sigma-Aldrich, St. Louis, MO) was injected and mice were euthanized 22-24 hours later. The ear was harvested, and Evans blue was extracted in 300μl formamide at 58°C overnight and quantified by absorbance using a Multiskan Ascent plate reader (Titertek, Pforzheim, Germany) at 620nm using a titration curve which was done in duplicates.

Flow cytometry staining and quantification

For staining of murine whole skin, single cell suspensions of skin were generated as previously described [34]. Ear skin was excised, finely minced, digested in collagenase type II (616 U/mL; Worthington Biochemical Corporation), dispase (2.42 U/mL; Life Technologies), and DNAse1 (80 μg/mL; Sigma-Aldrich), incubated at 37°C while shaking at 100 rpm, triturated with glass pipettes, and filtered.

For staining of whole lymph nodes, single cell suspensions were generated as previously described [35]. Lymph nodes were harvested, minced, and digested with type II collagenase (616 U/mL) and DNAase1 (40μg/mL), incubated at 37°C while shaking at 50 rpm, triturated with glass pipettes, and filtered.

For staining of non-stromal cells from the lymph node, whole lymph nodes were harvested and mashed through a 70um strainer. BD Cytofix/Cytoperm kit was used for intracellular staining.

For flow cytometry analysis, the following gating strategies were used after excluding debris, non-single cells, and dead cells using 4',6-diamidino-2-phenylindole dihydrochloride (DAPI) for non-fixed cells. All samples were treated with Fc block prior to antibody staining: B cells: CD45+ B220+; monocytes: CD45+, B220-, CD3-, CD11b+, Ly6C+; neutrophils: CD45+ CD11b+ Ly6Cmed, side scatter (SSC)hi or CD45+, CD11b+, Ly6Cmed, Ly6G+; T cells: CD45+, CD3+; germinal center B cells: CD3-, B220+, GL7+, PNA+; plasma cells: CD3-, B220med-lo, CD138+. In experiments that used digestion, plasmablasts were identified by intracellular IgG in lieu of CD138. Lymphatic endothelial cells: CD45-, CD31+, GP38+; fibroblastic reticular cell: CD45-, CD31-. GP38+. CCL2 was identified by either using CCL2-GFP reporter mice or by staining. Staining with CCL2 was done by staining with CCL2-FITC

and amplifying signal by staining with anti-FITC-biotin and subsequently SA-FITC. Negative control for GFP signal done by using C57Bl/6 mice in M1R experiments and by isotype control is experiments. $CCL2^{-/-}$ mice were used for negative control for staining experiments.

For flow cytometry analysis, cells were analyzed using a FACSCanto or FACSSymphony (BD Biosciences) and FlowJo Software (Tree Star).

Cells were counted using a Multisizer 4e Coulter Counter (Beckman Coulter). To calculate absolute cell numbers, the percentage of the total of a particular population was multiplied by the total cell count from the Coulter Counter.

Monocyte characteristics in transplanted lymph nodes were assessed from previously- performed experiments [12]. The data were from CCL2-/- popliteal lymph nodes transplanted into WT hosts and WT lymph nodes transplanted into WT hosts, immunized with ovalbumin/alum, and examined at day 12.

All antibodies and staining reagents are described in Table S1.

Statistics

For figures showing normalized values, the control sample was set to 1, and the experimental samples were normalized relative to the control for that experiment. For experiments that contained more than one control sample, the mean was obtained for the control samples, and the individual control and experimental samples were calculated relative to this mean.

Statistical significance was determined using 2-tailed unpaired Student's *t* test; $p<0.05$ was considered significant. Error bars represent standard deviation.

ACKNOWLEDGMENTS

The authors thank the Lu Lab for critical reading of the manuscript. This work was supported by National Institutes of Health grants R01AI079178 (TTL), Lupus Research Alliance (TTL), and the St. Giles Foundation (TTL). NIH Office of the Director grant S10OD019986 to Hospital for Special Surgery.

AUTHOR CONTRIBUTIONS

WGA, NS, and TTL conceived the study; WGA, MH, MLC, ESS, JS, JS, NS, DD, CC, RK designed and performed the experiments and analyzed the data, WDS, ES, DE, RK, and BM provided key reagents and intellectual input. CC and SR designed experiments and provided intellectual input. TTL designed, supervised, and interpreted experiments. WGA and TTL wrote the manuscript; all authors contributed to editing and manuscript revisions.

FIGURE LEGENDS

Figure 1. Patients with SLE and murine SLE models show signs of cutaneous lymphatic dysfunction

(A) Punch biopsies of skin from healthy control (HC), APL (without SLE), and SLE subjects were stained for CD31+PDPN+ lymphatic vessels. (A) Representative photomicrograph. Arrowheads point to lymphatic vessels. (B) Size of lymphatic vessels as indicated by CD31+PDPN+ area divided by the number of lymphatic vessels. Each symbol is an individual subject. (C) Number of lymphatic vessels per tissue area. (D-H) LPR and MRL controls were treated for UVR or examined at homeostasis and assessed for lymphatic function by Evans blue retention and ear swelling. (D) Experimental design for (E-F). (E) Relative retention of intradermally injected Evans blue in ear skin. (F) Relative ear thickness. (G-H) Homeostatic (G) Evans blue retention and (H) ear thickness. (I-K) IMQ lupus model was induced in B6 mice by topical application of IMQ on right ear and response to UVR in "non-lesional" left and "lesional" right ears were examined. (I) Experimental design. (J) Evans blue retention. (K) Ear swelling. Each symbol represents one mouse; n= 5 to 10 per condition; data are from 5 to 6 (D, E, J (left), K (left)), 4 (K (right)) and 3 (G, J (right)) independent experiments. ***P<0.001, **P<0.01, *P<0.05 by unpaired Student's *t* test. Error bars represent SD. NS, not significant.

Figure 2. Improving lymphatic flow reduces photosensitivity of skin in SLE models

(A-G) LPR mice and (H-M) B6 IMQ mice were treated with MLD on left ear or were handling controls during UVR treatment and skin responses examined. (A,H) Experimental design (B) Representative images of LPR ears at 24 hours after Evans blue injection with and without MLD. (C,I) Evans blue retention, (D,J) ear thickness , and (E,K) monocyte, (F,L) neutrophil, and (G,M)

T cell numbers in left ears with MLD relative to mice that did not receive MLD. (N-U) LEC^{PTEN} and LEC^{WT} mice were treated with IMQ on the right ear, treated with UVR and ear skin assessed, as in (N). (O) Evans blue retention, (P) ear thickness, (Q) monocytes, (R) neutrophils, and (S) T cells of the left and right ears, relative to ears of IMQ LEC^{WT} mice. Each symbol represents one mouse; n= 3 to 19 per condition; data are from 10 (E-G), 7 to 8 (C, D, J), 4 (K, L, M, P, Q, R, S), 3 (I, O) and 2 (T, U) independent experiments. ***P<0.001, **P<0.01, *P<0.05 by unpaired Student's *t* tests Error bars represent SD.

Figure 3. Improving lymphatic flow reduces draining lymph node B cell responses in SLE models

(A-F) Left auricular lymph nodes of (A-C) B6 IMQ mice treated with MLD or that were handling controls and (D-F) IMQ LEC^{PTEN} and IMQ LEC^{WT} mice were examined. (A,D) Lymph node cellularity. (B,E) B and T cell numbers and B:T cell ration. (C,F) Germinal center B cell and plasmablast numbers, relative to controls. (G) Relative splenic weight of IMQ LEC^{PTEN} and IMQ LEC^{WT} mice. Each symbol represents one mouse; n= 3 to 20 per condition; data are from 11 (A), 8 (D), and 5 to 6 (B, C, E, F, G), and 3 (C-germinal center B cell) independent experiments. ***P<0.001, **P<0.01, *P<0.05 by unpaired Student's *t* tests. Error bars represent SD.

Figure 4. Improving lymphatic flow increases lymph node FRC CCL2

(A-D,F) Left auricular lymph nodes of (A,C,D,F) IMQ-treated CCL2-GFP reporter mice treated with MLD or that were handling controls and (B) IMQ LEC^{PTEN} and IMQ LEC^{WT} mice were examined. (A-B) Representative histogram and graphical representation of FRC CCL2

expression. (C) LEC CCL2. (D) Ly6C^{hi} monocyte numbers per lymph node. (E) CD11b and forward scatter characteristics of Ly6C^{hi} monocytes from Ccl2-/- or WT lymph nodes that had been transplanted into WT hosts and then examined at day 15 after immunization with ovalbumin in alum [12] (F) CD11b and forward scatter characteristics of Ly6C^{hi} monocytes from B6 IMQ mice treated with MLD or subject to control handling. Each symbol represents one mouse; n= 5 to 14 per condition; data are from 7 (A, E), 5 (D, F), 4 (C), and 2 (B) independent experiments. **P<0.01, *P<0.05 by unpaired Student's *t* tests. Error bars represent SD.

Figure 5. Reduction of lymph node B cell responses with improved lymphatic flow is dependent on Gr-1+ cells

(A-D) B6 IMQ mice were treated with anti-Gr-1 or isotype control at days -1, 0, and+2 of UVR and MLD treatments as shown in (A), and left auricular lymph node examined. (B) Lymph node cellularity. (C) Germinal center B cell and (D) plasmablast numbers per lymph node, relative to isotype control-treated mice. Each symbol represents one mouse; n= 3 per condition; data are from 3 independent experiments. *P<0.05 by unpaired Student's *t* tests. Error bars represent SD.

SUPPLEMENTARY FIGURE LEGENDS

Fig S1. Characterization lymph node composition with tamoxifen treatment in B6 IMQ model

A. Total cells per lymph node. B. B/T cell ratio. C. Relative germinal center cell per lymph node. D. Relative plasmablasts per lymph node. Each symbol represents one mouse; n= 3 per condition; data are from 2 independent experiments. ***P<0.001, **P<0.01, *P<0.05 by unpaired Student's *t* tests. Error bars represent SD. ns, not significant.

Figure S2. Effects on lymph nodes after MLD in LPR mice

(A-C) LPR mice were treated with MLD or were handling controls during UVR and draining left auricular nodes examined. (A) Lymph node cellularity. (B) B and T cells per lymph node, and B:T cell ration. (C) Germinal center and plasmablast numbers , relative to handling controls. Each symbol represents one mouse; n= 3-16 per condition; data are from 12 (A), 11 (B, C, D, E), and 3 (F) independent experiments. ***P<0.001, **P<0.01, *P<0.05 by unpaired or paired Student's *t* tests when appropriate. Error bars represent SD. ns, not significant.

REFERENCES

1. Ahluwalia, J. and A. Marsch, *Photosensitivity and photoprotection in patients with lupus erythematosus.* Lupus, 2019. **28**(6): p. 697-702.
2. Kuhn, A., et al., *Photoprotective effects of a broad-spectrum sunscreen in ultraviolet-induced cutaneous lupus erythematosus: a randomized, vehicle-controlled, double-blind study.* J Am Acad Dermatol, 2011. **64**(1): p. 37-48.
3. Vilá, L.M., et al., *Association of sunlight exposure and photoprotection measures with clinical outcome in systemic lupus erythematosus.* P R Health Sci J, 1999. **18**(2): p. 89-94.
4. Mikita, N., et al., *Recent advances in cytokines in cutaneous and systemic lupus erythematosus.* J Dermatol, 2011. **38**(9): p. 839-49.
5. Ogunsanya, M.E., et al., *A systematic review of patient-reported outcomes in patients with cutaneous lupus erythematosus.* Br J Dermatol, 2017. **176**(1): p. 52-61.
6. Tebbe, B. and C.E. Orfanos, *Epidemiology and socioeconomic impact of skin disease in lupus erythematosus.* Lupus, 1997. **6**(2): p. 96-104.
7. Sim, J.H., et al., *Immune Cell–Stromal Circuitry in Lupus Photosensitivity.* The Journal of Immunology, 2021. **206**(2): p. 302-309.
8. Kahlenberg, J.M., *Rethinking the Pathogenesis of Cutaneous Lupus.* J Invest Dermatol, 2021. **141**(1): p. 32-35.
9. Patel, J., R. Borucki, and V.P. Werth, *An Update on the Pathogenesis of Cutaneous Lupus Erythematosus and Its Role in Clinical Practice.* Curr Rheumatol Rep, 2020. **22**(10): p. 69.
10. Thomas, S.N., et al., *Impaired Humoral Immunity and Tolerance in K14-VEGFR-3-Ig Mice That Lack Dermal Lymphatic Drainage.* The Journal of Immunology, 2012. **189**(5): p. 2181-2190.
11. Kajiya, K. and M. Detmar, *An Important Role of Lymphatic Vessels in the Control of UVB-Induced Edema Formation and Inflammation.* J Invest Dermatol, 2006. **126**(4): p. 920-922.
12. Dasoveanu, D.C., et al., *Lymph node stromal CCL2 limits antibody responses.* Sci Immunol, 2020. **5**(45).
13. Yazici, Y., et al., *Protein-losing enteropathy in systemic lupus erythematosus: report of a severe, persistent case and review of pathophysiology.* Lupus, 2002. **11**(2): p. 119-123.
14. von der Weid, P.-Y., S. Rehal, and J.G.P. Ferraz, *Role of the lymphatic system in the pathogenesis of Crohn's disease.* Current Opinion in Gastroenterology, 2011. **27**(4).
15. Rossi, A., et al., *Lymphatic and blood vessels in scleroderma skin, a morphometric analysis.* Human Pathology, 2010. **41**(3): p. 366-374.
16. Sevim, E., et al., *Mammalian Target of Rapamycin Pathway Assessment in Antiphospholipid Antibody Positive Patients with Livedo.* J Rheumatol, 2022.
17. Huggenberger, R., et al., *An important role of lymphatic vessel activation in limiting acute inflammation.* Blood, 2011. **117**(17): p. 4667-4678.
18. Yokogawa, M., et al., *Epicutaneous application of toll-like receptor 7 agonists leads to systemic autoimmunity in wild-type mice: a new model of systemic Lupus erythematosus.* Arthritis Rheumatol, 2014. **66**(3): p. 694-706.
19. Furukawa, F., *Photosensitivity in cutaneous lupus erythematosus: lessons from mice and men.* J Dermatol Sci, 2003. **33**(2): p. 81-9.
20. Shipman, W.D., et al., *A protective Langerhans cell-keratinocyte axis that is dysfunctional in photosensitivity.* Sci Transl Med, 2018. **10**(454).
21. Klionsky, D.J., et al., *Guidelines for the use and interpretation of assays for monitoring autophagy (3rd edition).* Autophagy, 2016. **12**(1): p. 1-222.

22. Lurie, F., et al., *The American Venous Forum, American Vein and Lymphatic Society and the Society for Vascular Medicine expert opinion consensus on lymphedema diagnosis and treatment.* Phlebology, 2022. **37**(4): p. 252-266.
23. Kataru, R.P., et al., *Lymphatic-specific intracellular modulation of receptor tyrosine kinase signaling improves lymphatic growth and function.* Sci Signal, 2021. **14**(695).
24. Huggenberger, R., et al., *Stimulation of lymphangiogenesis via VEGFR-3 inhibits chronic skin inflammation.* J Exp Med, 2010. **207**(10): p. 2255-69.
25. Schwager, S., et al., *Antibody-mediated delivery of VEGF-C potently reduces chronic skin inflammation.* JCI Insight, 2018. **3**(23).
26. Angeli, V., et al., *B cell-driven lymphangiogenesis in inflamed lymph nodes enhances dendritic cell mobilization.* Immunity, 2006. **24**(2): p. 203-15.
27. Chyou, S., et al., *Normalization of the lymph node T cell stromal microenvironment in lpr/lpr Mice is associated with SU5416-induced reduction in autoantibodies.* PLoS ONE, 2012. **7**(3): p. e32828.
28. Liu, Y., et al., *Accelerated model of lupus autoimmunity and vasculopathy driven by toll-like receptor 7/9 imbalance.* Lupus Science & Medicine, 2018. **5**(1): p. e000259.
29. Tomei, A.A., et al., *Fluid flow regulates stromal cell organization and CCL21 expression in a tissue-engineered lymph node microenvironment.* J Immunol, 2009. **183**(7): p. 4273-83.
30. Lu, B., et al., *Abnormalities in monocyte recruitment and cytokine expression in monocyte chemoattractant protein 1-deficient mice.* J Exp Med, 1998. **187**(4): p. 601-8.
31. Shi, C., et al., *Bone marrow mesenchymal stem and progenitor cells induce monocyte emigration in response to circulating toll-like receptor ligands.* Immunity, 2011. **34**(4): p. 590-601.
32. Kataru, R.P., et al., *Lymphatic-specific intracellular modulation of receptor tyrosine kinase signaling improves lymphatic growth and function.* Science Signaling, 2021. **14**(695): p. eabc0836.
33. Escobedo, N., et al., *Restoration of lymphatic function rescues obesity in Prox1-haploinsufficient mice.* JCI Insight, 2016. **1**(2).
34. Chia, J.J., et al., *Dendritic cells maintain dermal adipose-derived stromal cells in skin fibrosis.* J Clin Invest, 2016. **126**(11): p. 4331-4345.
35. Chyou, S., et al., *Coordinated regulation of lymph node vascular-stromal growth first by CD11c+ cells and then by T and B cells.* J Immunol, 2011. **187**(11): p. 5558-67.

Figure 1

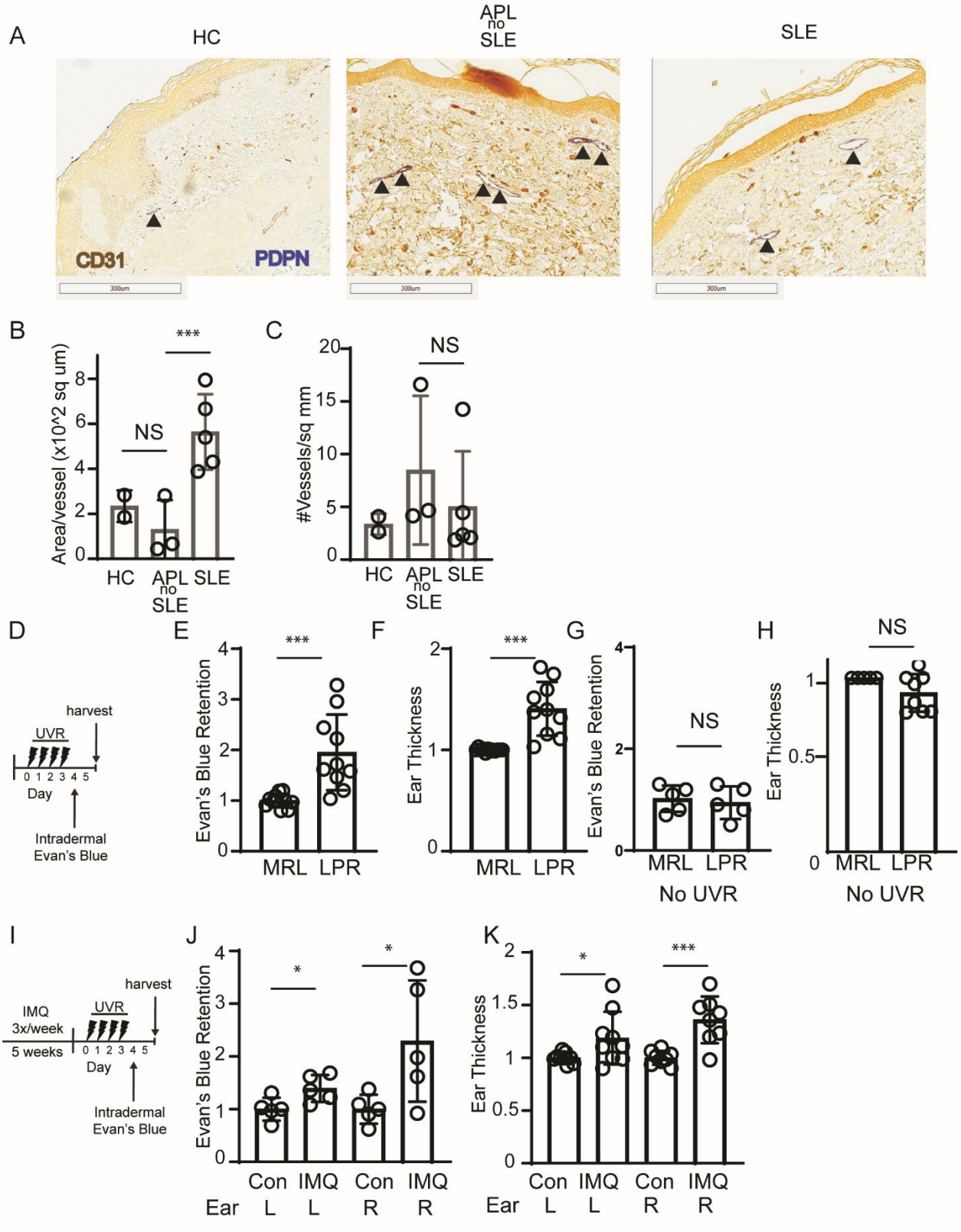
A
HC
APL no SLE
SLE
CD31
PDPN
300um
B
Area/vessel (x10^2 sq um)
NS
***
HC
APL no SLE
SLE
C
#Vessels/sq mm
NS
D
harvest
UVR
0 1 2 3 4 5
Day
Intradermal Evan's Blue
E
Evan's Blue Retention
***
MRL
LPR
F
Ear Thickness
***
G
Evan's Blue Retention
NS
No UVR
H
Ear Thickness
NS
I
IMQ 3x/week
5 weeks
harvest
UVR
Day
Intradermal Evan's Blue
J
Evan's Blue Retention
*
*
Con IMQ Con IMQ
Ear L L R R
K
Ear Thickness
*
***

Figure 2

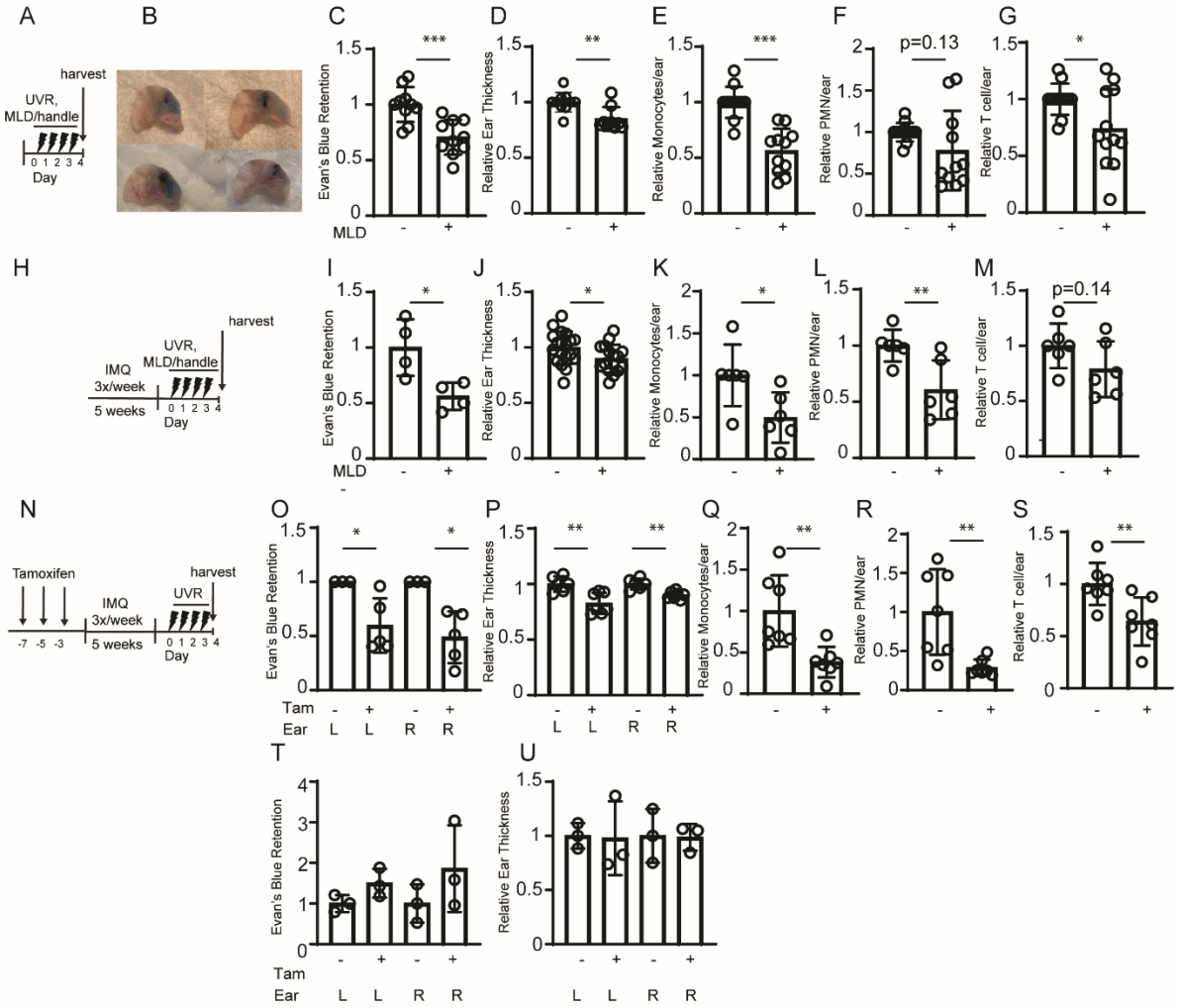
A
B
C
D
E
F
G
H
I
J
K
L
M
N
O
P
Q
R
S
T
U
harvest
UVR,
MLD/handle
0 1 2 3 4
Day
IMQ
3x/week
5 weeks
Tamoxifen
-7 -5 -3
UVR
Evan's Blue Retention
Relative Ear Thickness
Relative Monocytes/ear
Relative PMN/ear
Relative T cell/ear
MLD
Tam
Ear
L L R R
p=0.13
p=0.14

Figure 3

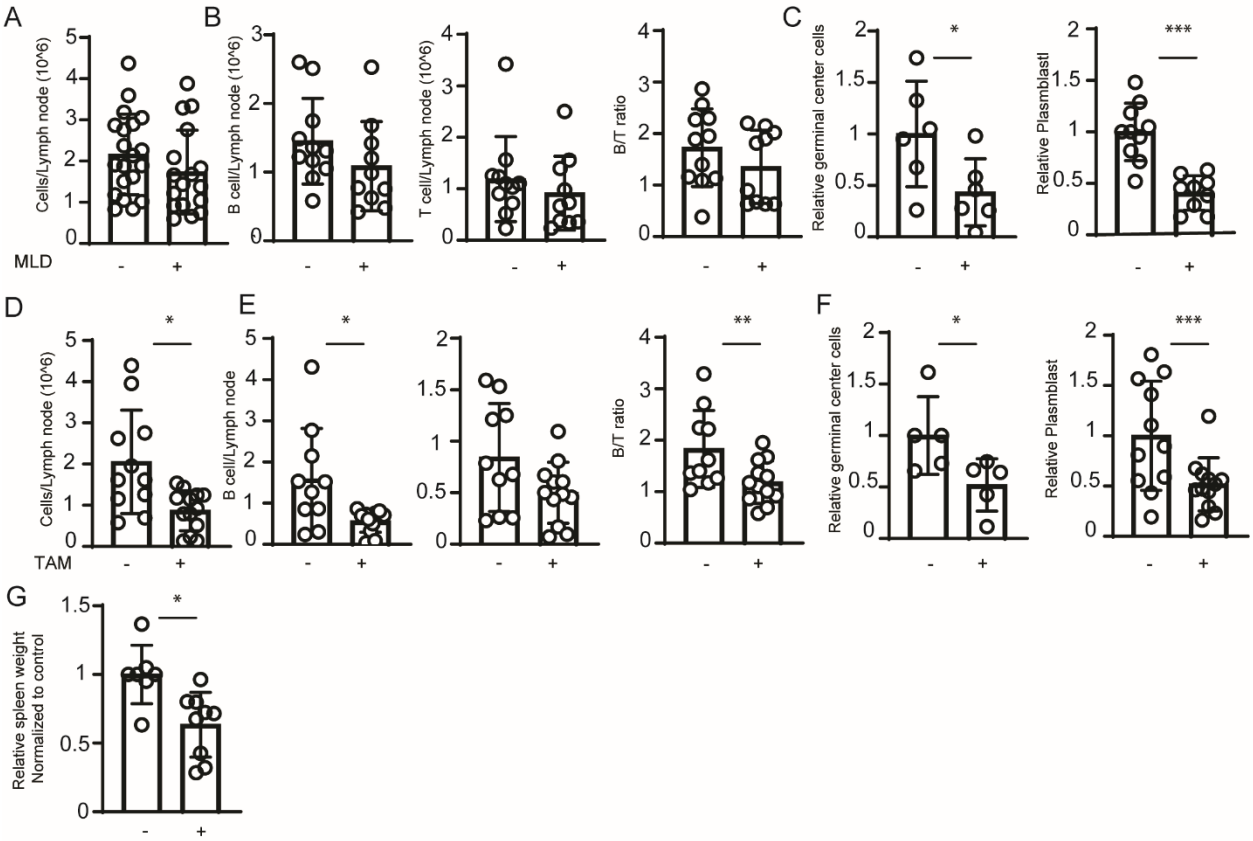
A
Cells/Lymph node (10^6)
MLD
B
B cell/Lymph node (10^6)
T cell/Lymph node (10^6)
B/T ratio
C
Relative germinal center cells
Relative Plasmblastl
D
Cells/Lymph node (10^6)
TAM
E
B cell/Lymph node
B/T ratio
F
Relative germinal center cells
Relative Plasmblast
G
Relative spleen weight
Normalized to control

Figure 4

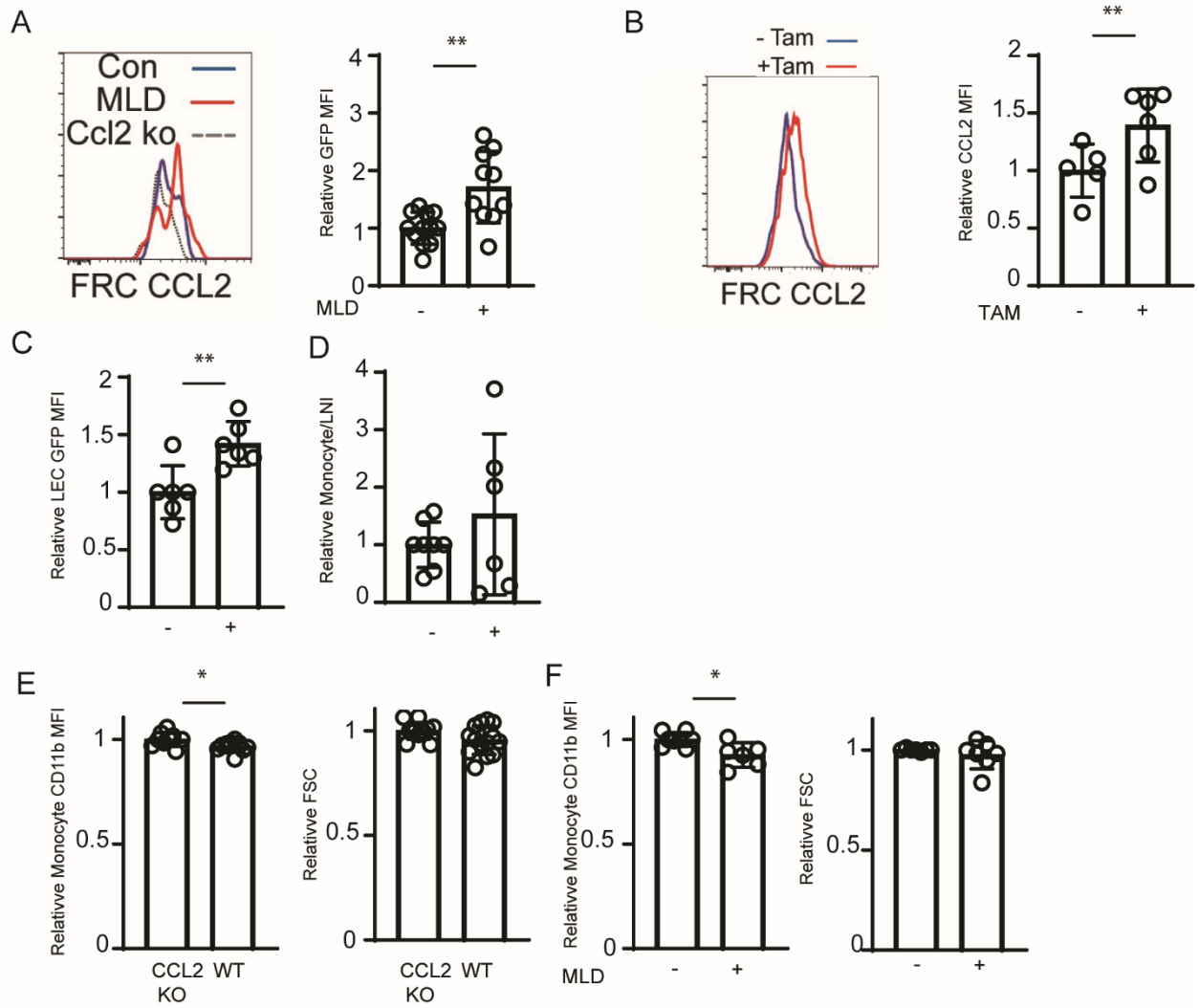
A
Con
MLD
Ccl2 ko
FRC CCL2
Relativve GFP MFI
MLD
-
+
**
B
- Tam
+Tam
FRC CCL2
Relativve CCL2 MFI
TAM
-
+
**
C
Relativve LEC GFP MFI
**
D
Relativve Monocyte/LNI
E
Relativve Monocyte CD11b MFI
CCL2 KO
WT
*
Relativve FSC
F
Relativve Monocyte CD11b MFI
MLD
*
Relativve FSC

Figure 5

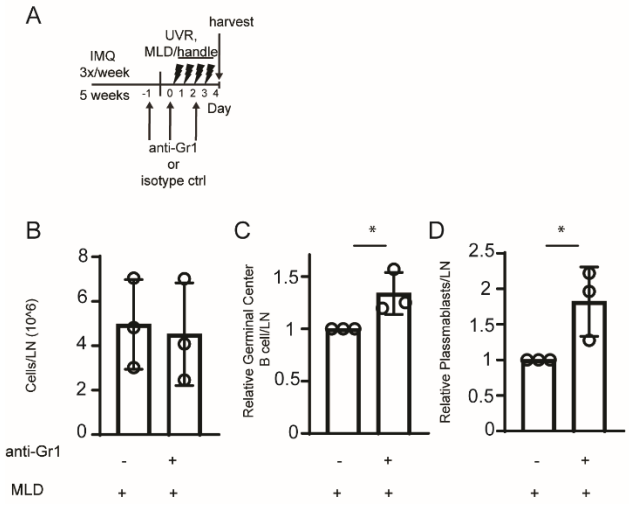
A
harvest
UVR,
MLD/handle
IMQ
3x/week
5 weeks
-1 0 1 2 3 4
Day
anti-Gr1
or
isotype ctrl
B
Cells/LN (10^6)
8
6
4
2
0
anti-Gr1
-
+
MLD
+
+
C
*
Relative Germinal Center B cell/LN
1.5
1
0.5
0
-
+
+
+
D
*
Relative Plasmablasts/LN
2.5
2
1.5
1
0.5
0
-
+
+
+

Figure S1

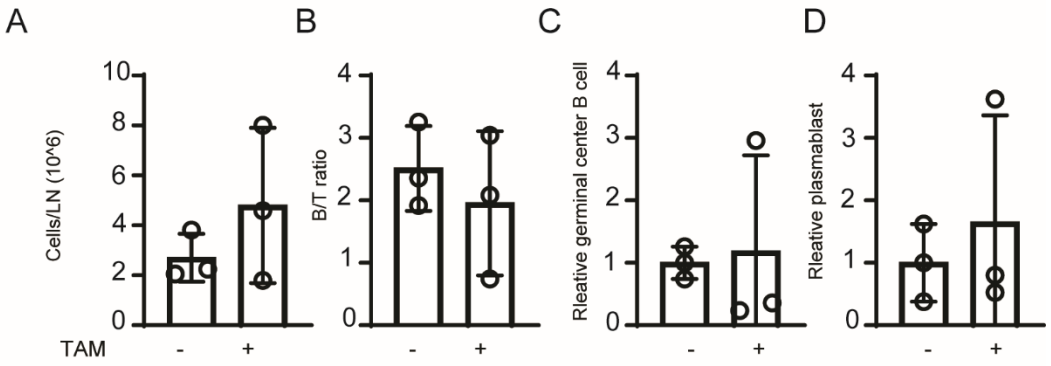
A
B
C
D
Cells/LN (10^6)
B/T ratio
Rleative germinal center B cell
Rleative plasmablast
TAM
-
+

Figure S2

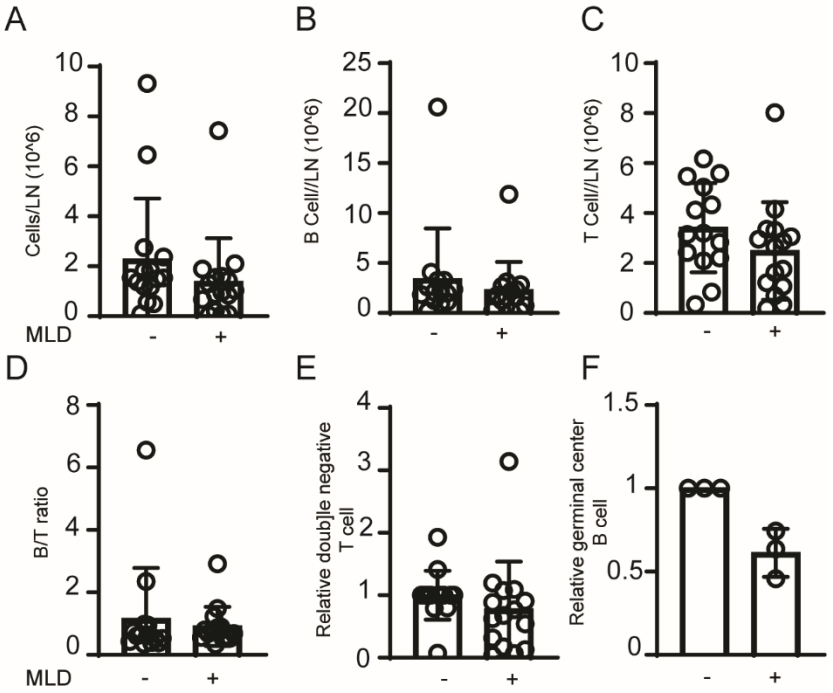
A
Cells/LN (10^6)
10
8
6
4
2
0
MLD
-
+
B
B Cell//LN (10^6)
25
20
15
10
5
0
-
+
C
T Cell//LN (10^6)
10
8
6
4
2
0
-
+
D
B/T ratio
8
6
4
2
0
MLD
-
+
E
Relative doub]le negative T cell
4
3
2
1
0
-
+
F
Relative germinal center B cell
1.5
1
0.5
0
-
+